Vector-Controlled Grid Synchronization for the Brushless Doubly-Fed Induction Generator

Alexander Broekhof, Mark Tatlow and Richard McMahon

Department of Engineering, University of Cambridge, Cambridge, UK, CB2 1PZ, Email: ab940@cam.ac.uk

Abstract. To further demonstrate the applicability of the brushless doubly-fed induction generator to wind turbine applications, a grid synchronization procedure is developed. Vector control of the converter-side stator winding is used to induce a voltage on the grid-side stator winding. A detector is developed to automatically connect the machine to the grid when the voltages are synchronized. Experimental results show that synchronization occurs within 0.4 seconds while the rotor is accelerating.

1. Introduction

The brushless doubly-fed induction generator (BDFIG) shows promise for use as a generator in wind turbines [1]. Its dual stator windings, the power winding (PW) and control winding (CW), allow variable-speed operation with a fractionally-rated voltage converter, while increasing reliability through the elimination of slip-rings and brush gear.

A further requirement for the BDFIG to be deployed in wind applications is the ability to quickly and safely connect to the grid when the cut-in wind speed is reached. For the connection to occur, the PW voltage must have equal amplitude, phase and frequency to the grid voltage. As the BDFIG rotor is designed to couple with both the PW and CW, it is possible to create these conditions on the PW by controlling the CW current.

Grid synchronization for the BDFIG has been demonstrated using vector control in [2,3]. Direct power control was used to synchronize the cascaded brushless doubly-fed induction generator, a very similar machine to the BDFIG, in [4]. However, in none of these works were experimental results provided.

In this paper a vector control method is used to synchronize a physical D180 frame size BDFIG. Additionally, it is shown that the control scheme is able to synchronize while the rotor is accelerating. Once the PW is connected to the grid, the controller is switched to use active/reactive power references to resume normal operation of the BDFIG.

2. Vector control for the BDFIG

The PW and CW have unequal pole-pair numbers, p_1 and p_2 respectively, to prevent their coupling directly. One possible way for the rotor to couple with both windings is to have $p_1 + p_2$ sets of nested loops [5]. With this setup, the BDFIG operates in a synchronous mode of operation which is dictated by the following relationship:

$$\omega_r = \frac{\omega_1 + \omega_2}{p_1 + p_2} \tag{1}$$

where $\omega_r (\mathrm{rad\,s^{-1}})$ is rotor angular velocity and $\omega_1, \omega_2 (\mathrm{rad\,s^{-1}})$ are the frequencies of the PW and CW.

When the PW is open-circuited, the frequency of the induced voltage is then governed by:

$$\omega_1 = (p_1 + p_2)\omega_r - \omega_2 \tag{2}$$

Therefore, to ensure that $\omega_1 = \omega_g$, set:

$$\omega_2 = (p_1 + p_2)\omega_r - \omega_g \tag{3}$$

It is shown in [6] that machine quantities will be constant in the steady-state if they are transformed to a unified reference frame (expressed in terms of a p_1 pole-pair distribution). The transformation to convert CW dq quantities to the stationary $\alpha\beta$ reference frame is given by:

$$\vec{x}_{\alpha\beta_2} = e^{j((p_1+p_2)\theta_r - p_2\gamma - \theta_a)}\vec{x}^*_{dq} \tag{4}$$

where superscript $*$ denotes a complex-conjugate, γ is a machine-dependent parameter, $\vec{x}_{dq} = x_{2d} + jx_{2q}$, and θ_a is an arbitrary reference frame. Differentiating the argument of eq. (4) produces:

$$\tfrac{\mathrm{d}}{\mathrm{d}t}((p_1 + p_2)\theta_r - p_2\gamma - \theta_a) = (p_1 + p_2)\omega_r - \omega_a \tag{5}$$

Therefore, by setting θ_a to the angle of the grid voltage vector (θ_g), applying constant dq inputs to the CW will ensure that eq. (3) is satisfied and that $\omega_1 = \omega_g$.

The grid synchronization process can then be expressed as a phase-lock loop (PLL). With the dq reference frame aligned with θ_g:

$$v_{gd} = |V_g^{abc}| \tag{6}$$

$$v_{gq} = 0 \tag{7}$$

Therefore, grid synchronization is achieved when $\vec{v}_{1dq} = \vec{v}_{gdq}$.

2.1 Modeling BDFIG with open-circuited PW

A dynamic model of the BDFIG expressed as dq vector quantities in a unified reference frame is given by [6]:

$$\vec{v}_1 = R_1\vec{\imath}_1 + s\vec{\Psi}_1 + j\omega_g\vec{\Psi}_1 \tag{8}$$
$$\vec{\Psi}_1 = L_1\vec{\imath}_1 + L_{1r}\vec{\imath}_r \tag{9}$$
$$\vec{v}_r = R_r\vec{\imath}_r + s\vec{\Psi}_r + j(\omega_g - p_1\omega_r)\vec{\Psi}_r \tag{10}$$
$$\vec{\Psi}_r = L_{1r}\vec{\imath}_1 + L_{2r}\vec{\imath}_2 + L_r\vec{\imath}_r \tag{11}$$
$$\vec{v}_2 = R_2\vec{\imath}_2 + s\vec{\Psi}_2 + j(\omega_g - (p_1+p_2)\omega_r)\vec{\Psi}_2 \tag{12}$$
$$\vec{\Psi}_2 = L_2\vec{\imath}_2 + L_{2r}\vec{\imath}_r \tag{13}$$

As the rotor is composed of short-circuited nested loops, there is no voltage across its windings. Additionally, before grid synchronization occurs, the PW phases are open circuited, thereby preventing current from flowing. Under these conditions, eqs. (8) to (13) become:

$$\vec{v}_1 = sL_{1r}\vec{\imath}_r + j\omega_g L_{1r}\vec{\imath}_r \tag{14}$$
$$\vec{0} = R_r\vec{\imath}_r + s(L_{2r}\vec{\imath}_2 + L_r\vec{\imath}_r) + j(\omega_g - p_1\omega_r)(L_{2r}\vec{\imath}_2 + L_r\vec{\imath}_r) \tag{15}$$
$$\vec{v}_2 = R_2\vec{\imath}_2 + s(L_2\vec{\imath}_2 + L_{2r}\vec{\imath}_r) + j(\omega_g - (p_1+p_2)\omega_r)(L_2\vec{\imath}_2 + L_{2r}\vec{\imath}_r) \tag{16}$$

With the PW disconnected, eqs. (14) to (16) resemble the equations for the standard induction machine. In fact, the BDFIG will operate (albeit, poorly) as a p_1 or p_2 pole-pair induction machine when either the CW or PW is open-circuited.

Splitting eqs. (14) to (16) into dq components produces:

$$v_{1d} = sL_{1r}i_{rd} - \omega_g L_{1r}i_{rq} \tag{17}$$
$$v_{1q} = sL_{1r}i_{rq} + \omega_g L_{1r}i_{rd} \tag{18}$$
$$0 = R_r i_{rd} + s(L_{2r}i_{2d} + L_r i_{rd}) - (\omega_g - p_1\omega_r)(L_{2r}i_{2q} + L_r i_{rq}) \tag{19}$$
$$0 = R_r i_{rq} + s(L_{2r}i_{2q} + L_r i_{rq}) + (\omega_g - p_1\omega_r)(L_{2r}i_{2d} + L_r i_{rd}) \tag{20}$$
$$v_{2d} = R_2 i_{2d} + s(L_2 i_{2d} + L_{2r}i_{rd}) - (\omega_g - (p_1+p_2)\omega_r)(L_2 i_{2q} + L_{2r}i_{rq}) \tag{21}$$
$$v_{2q} = R_2 i_{2q} + s(L_2 i_{2q} + L_{2r}i_{rq}) + (\omega_g - (p_1+p_2)\omega_r)(L_2 i_{2d} + L_{2r}i_{rd}) \tag{22}$$

As rotor speed is controlled via an external system (blade actuators in the case of a wind turbine), ω_r is regarded as a time-varying parameter. Therefore, eqs. (17) to (22) form a system of six equations with eight variables.

2.2 Input-output pairing using relative gain arrays

Solving eqs. (17) to (22) for six of the eight variables produces a set of multi-input, multi-output (MIMO) transfer functions which can be used to determine the input-output relations in the system. For the purposes of grid synchronization with cascaded controllers, the important relations are:

$$\vec{v}_{2dq} \rightarrow \vec{\imath}_{2dq} \rightarrow \vec{v}_{1dq} \tag{23}$$

These relations can be expressed in transfer matrix form as:

$$\begin{bmatrix} i_{2d} \\ i_{2q} \end{bmatrix} = \begin{bmatrix} G_{1,1}(s) & G_{1,2}(s) \\ G_{2,1}(s) & G_{2,2}(s) \end{bmatrix} \begin{bmatrix} v_{2d} \\ v_{2q} \end{bmatrix} \tag{24}$$
$$\begin{bmatrix} v_{1d} \\ v_{1q} \end{bmatrix} = \begin{bmatrix} H_{1,1}(s) & H_{1,2}(s) \\ H_{2,1}(s) & H_{2,2}(s) \end{bmatrix} \begin{bmatrix} i_{2d} \\ i_{2q} \end{bmatrix} \tag{25}$$

The input-output pairings can be determined using the relative gain array (RGA), defined for G as:

$$\mathrm{RGA}(G) = (G(0)^{-1})^T \cdot G(0) \tag{26}$$

where $\cdot$ represents element-wise multiplication. Numerically solving eqs. (17) to (22) using the parameters listed in table 1 (derived from the machine specified in table 2) and evaluating the the RGA at natural speed ($\omega_r = \frac{100\pi}{6}$) gives:

$$\mathrm{RGA}(G) = \begin{bmatrix} 0.9998 & 0.0002 \\ 0.0002 & 0.9998 \end{bmatrix} \tag{27}$$
$$\mathrm{RGA}(H) = \begin{bmatrix} 1.0084 & -0.0084 \\ -0.0084 & 1.0084 \end{bmatrix} \tag{28}$$

The input-output pairing is chosen by selecting the largest value in each row of the RGA. From eqs. (27) and (28), it is clear that the pairings should be:

$$v_{2d} \rightarrow i_{2d} \rightarrow v_{1d} \tag{29}$$
$$v_{2q} \rightarrow i_{2q} \rightarrow v_{1q} \tag{30}$$

A control system can then be established using PI controllers, as shown in fig. 1.

It has been shown in [7] that when controlling active and reactive power in the BDFIG, the relationships:

$$\vec{v}_{2dq} \rightarrow \vec{\imath}_{2dq} \tag{31}$$

Table 1. BDFIG vector model parameters.

R_1	PW resistance	2.3 Ω
R_2	CW resistance	4.0 Ω
R_r	Rotor resistance	129.7 µΩ
L_1	PW self-inductance	349.8 mH
L_2	CW self-inductance	363.7 mH
L_r	Rotor self-inductance	44.5 µH
L_{1r}	PW-rotor mutual inductance	3.1 mH
L_{2r}	CW-rotor mutual-inductance	2.2 mH
p_1	PW pole-pairs	2
p_2	CW pole-pairs	4
ω_1	PW input frequency	50 Hz

will vary with rotor speed. By calculating eqs. (27) and (28) at various rotor speeds, it is clear that this parameter-varying coupling exists also when the PW is open-circuited. However, by tuning the PI controllers somewhat conservatively, synchronization is entirely feasible. Improved performance may be achieved with a decoupling network, but as the time spent in grid synchronization mode accounts for a minimal portion of a generator's lifespan, the added complexity is typically not merited.

2.3 Synchronization detection

A detector is needed to determine whether the PW voltage is tracking the grid voltage so that the contactor can be closed, connecting the BDFIG to the grid. As the detector must rely on the errors of two measurements, $e_{v_{1d}}$ and $e_{v_{1q}}$, they are combined using a 2-norm:

$$\|e_{\vec{v}_{1dq}}\|_2 = (e_{v_{1d}}^2 + e_{v_{1q}}^2)^{\frac{1}{2}} \tag{32}$$

However, this measurement is susceptible to noise and transient behavior. To determine whether the system has reached steady state, the error is filtered with a first-order low-pass filter with a $30\,\mathrm{rad\,s^{-1}}$ cutoff frequency. Due to the noise in the system, this mean will not reach zero, so a threshold is chosen which represents a sufficient level of tracking. To prevent chattering, a hysteresis relay is used to transmit the signal to the contactor.

2.4 Post-synchronization

Once the BDFIG is connected to the grid, the controller must immediately switch to regulation of active and reactive power. This is accomplished by changing the reference and measurement signals on the outer loop controller. As the magnitude of the power signals are orders of magnitude larger than the $\vec{v}_{1dq}$ signals, the gains of the outer loop PI controllers must also be altered.

3. Implementation

The grid synchronization method has been implemented on a BDFIG with specifications listed in table 2. The BDFIG is connected to a DC motor to act as the prime mover. In practical applications, the synchronization will occur when the generator is accelerating to its operating speed. In this implementation, the acceleration was set to $120\,\mathrm{rpm\,s^{-1}}$. The rotor speed curve profile is shown in fig. 2

However, the partially-rated voltage converter restricts the BDFIG to a operating region of $\omega_n \pm 30\%$. Additionally, it was found that the synchronization procedure experienced problems at lower end of the operating region. Therefore, synchronization was initiated once the rotor speed reached 450 rpm ($\omega_n - 10\%$).

The results of this synchronization are shown in fig. 3.

Table 2. BDFIG prototype specifications.

Frame size	D180
p_1	2
p_2	4
Stator slots	48
Rotor slots	36
PW rated voltage	240 V (RMS at 50 Hz)
CW rated voltage	240 V (RMS at 50 Hz)
PW rated current	7 A (RMS)
CW rated current	7 A (RMS)
Rated torque	100 N m
Rotor design	Nested-loop: 6, 3-loop nests

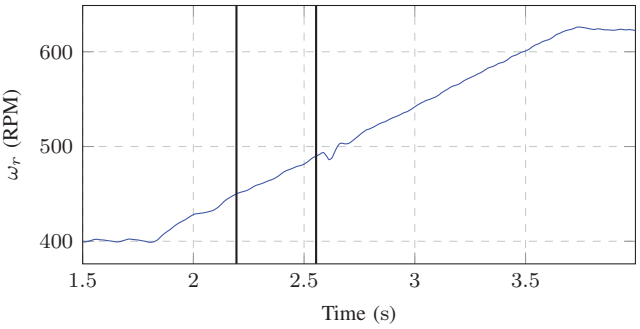

Figure 2. Rotor speed profile for experimental grid synchronization. First vertical line indicates start of grid synchronization routine. The second indicates the point of synchronization.

Figure 3a shows the a-phase voltages of the grid and PW. The PW voltage is initially noisy due to the high switching frequency of the inverter as it attempts to impose a zero voltage across the CW. However, the noise diminishes as the amplitude increases and good synchronization is achieved within 0.4 s.

The voltages in the dq reference frame are shown in fig. 3b. The coupling between the $\vec{v}_{2dq}$ and $\vec{v}_{1dq}$ axes is noticeable here, as increasing v_{1d} also leads to changes in v_{1q}. However, the PI controllers are able to account for this cross-coupling, and v_{1q} is regulated back to zero.

Also visible in this plot is the propagation delay of the contactor signal. While the contactor is activated at 2.554 s, the grid connection is not established until approximately 25 ms later. At this point, the error has actually increased again due to overshoot in the controller. While synchronizing at this level of error doe not significantly affect the machine, it is important to recognize that this is type of behavior is potentially problematic.

In fig. 3c, the filtered errors of the $\vec{v}_{1dq}$ signals are shown, as well as their 2-norm. Despite the increase in v_{1q} error, the 2-norm decreases monotonically to the contactor threshold of 39 V. This plot also demonstrates the effects of filter choice for the error norm. The $\vec{v}_{1dq}$ signals reach their minimum at approximately 2.54 s, however, due to delay in the filter, the 2-norm does not obtain its

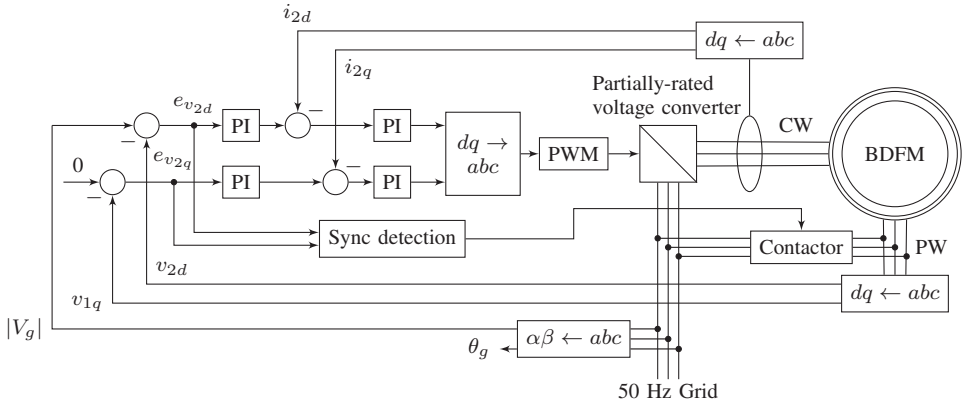

Figure 1. Grid synchronization setup

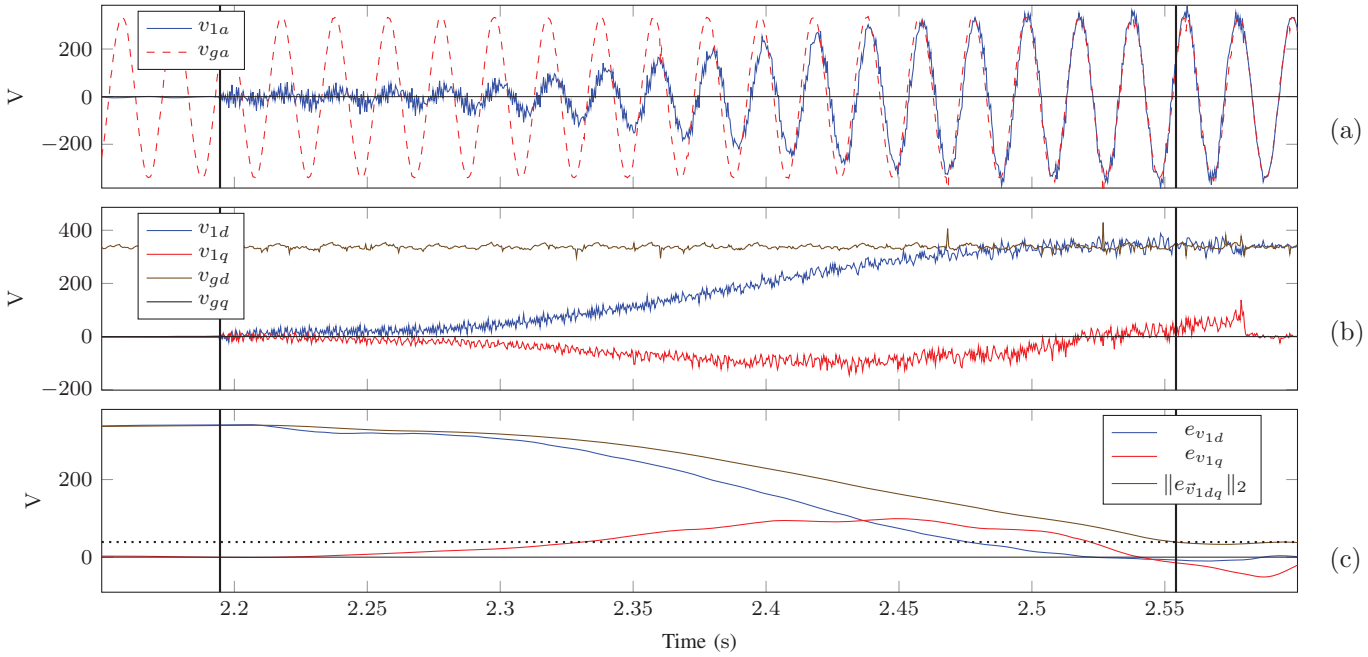

Figure 3. Experimental results

minimum until approximately 10 ms later. This also contributes to the delay between activating the contactor and the moment of grid connection.

In fig. 4, the a-phase currents of the PW and CW are shown over a longer time scale. When the synchronization procedure begins, the amplitude of i_2 increases to induce the voltage in the PW, but does not go above the rated current of the CW (7 A RMS ≈ 9.9 A amplitude). Interestingly, a current also appears on the PW prior to its being connected to the grid. This is likely a combination of sensor noise and the effects of any imbalances in the three-phases.

As in fig. 3, the actual grid connection occurs approximately 0.004 ms after the signal is sent. At this time, a current transient occurs on both the CW and PW, reaching a maximum of approximately 4 A. Following this transient, the currents of both windings go to their steady waveforms.

4. Conclusion

This paper has presented a control system which synchronizes a prototype BDFIG with the grid voltage within 0.4 s. Additionally, this synchronization is accomplished while the rotor speed is changing, showing that the control is valid at a range of speeds. By demonstrating fast and reliable synchronization, these experimental results support the application of the BDFIG to wind turbines.

Acknowledgements

This work has been supported by the EPSRC Control For Energy and Sustainability Grant and the Windrive consortium.

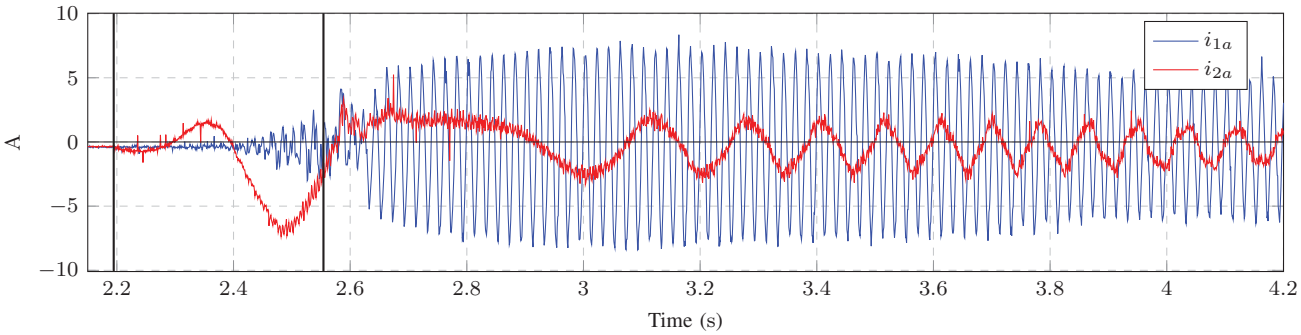

Figure 4. *a*-phase currents for the PW and CW

References

[1] R. McMahon, X. Wan, E. Abdi, P. J. Tavner, P. C. Roberts, and M. Jagiela, "The BDFM as a generator in wind turbines," in *12th International Power Electronics and Motion Control Conference*, August 2006, pp. 1859–1865.

[2] H. Voltolini and R. Carlson, "Grid synchronization and maximum power point tracking for wind energy generation system with brushless doubly fed induction generator," in *34th Annual Conference of IEEE Industrial Electronics*, 2008.

[3] K. Ji, S. Huang, J. Zhu, Y. Gao, and C. Zeng, "Vector control and synchronization of brushless doubly-fed machine for high power vector control and synchronization of brushless doubly-fed machine for high power wind power generation," in *15th International Conference on Electrical Machines and Systems*, 2012.

[4] Y. Zhang and J. Zhu, "Direct torque control of cascaded brushless doubly fed induction generator for wind energy applications," in *IEEE International Electric Machines and Drives Conference*, 2011.

[5] P. C. Roberts, "A study of brushless doubly-fed (induction) machines," Ph.D. dissertation, University of Cambridge, September 2004.

[6] J. Poza, E. Oyarbide, D. Roye, and M. Rodriguez, "Unified reference frame dq model of the brushless doubly fed machine," in *IET Proceedings Electric Power Applications*, vol. 153, no. 5. IET, September 2006.

[7] A. Broekhof, "Analysis of stator-flux-oriented vector control for the brushless doubly-fed machine," Master's thesis, University of Cambridge, 2012.